

Dynamic structure factor $S(\mathbf{k}, \omega)$ of beryllium by x-ray inelastic scattering experiments

A. Vradis and G. D. Priftis

Department of Physics, University of Patras, Patras, Greece

(Received 26 September 1984)

The dynamic structure factor $S(\mathbf{k}, \omega)$ of beryllium is determined by inelastic x-ray scattering experiments for a wide region of momentum transfer \mathbf{k} . The results show that the dispersion curve deviates from random-phase-approximation (RPA) predictions, especially for $k > k_c$, while for $k > k_F$ it splits into two branches. The lower branch, corresponding to the plasmonlike component, shows a negative slope for $0.9k_F < k < 1.5k_F$, whereas for greater values of k it remains nondispersive. The upper branch shows considerable dispersion and tends to become parallel to the recoil energy curve. The observed deviations from RPA can be attributed to short-range correlation effects and the existence of higher-order excitations according to the theory of Awa *et al.*

INTRODUCTION

The dynamic structure factor $S(\mathbf{k}, \omega)$ for electrons of simple metals has been the subject of extensive theoretical and experimental work.¹⁻³

Experimental methods for the study of $S(\mathbf{k}, \omega)$ are based on scattering experiments using either fast electrons or x rays. In such scattering experiments the incident beam interacts with the scatterer with a consequent transfer of momentum $\hbar\mathbf{k}$ and energy $\hbar\omega$. The differential cross section according to the Born approximation, for the case of x rays is

$$\frac{d^2\sigma}{d\Omega d\omega} = \left[\frac{e^2}{mc^2} \right]^2 (\mathbf{e}_1 \cdot \mathbf{e}_2)^2 \frac{\omega_2}{\omega_1} S(\mathbf{k}, \omega), \quad (1)$$

where $(e^2/mc^2)^2$ is the Rayleigh-Thompson scattering cross section, \mathbf{e}_1, ω_1 and \mathbf{e}_2, ω_2 are the polarization vector and the frequency of the incident and scattered x ray, respectively, with $\omega_2 \simeq \omega_1$ in the present case. $S(\mathbf{k}, \omega)$ is the dynamic structure factor, which contains the maximum possible information that can be obtained from any scattering experiment and is the Fourier transform of the space- and time-dependent density-density correlation function. It thus furnishes a direct measure of the density-fluctuation spectrum of the electrons of the scatterer.

As is well known, according to random-phase-approximation (RPA) theory,¹ plasmons exist when k is smaller than a critical wave vector k_c , which determines the limit between collective mode and single-particle excitations. In the region $k < k_c$ the dynamic structure factor $S(\mathbf{k}, \omega)$ is separated into two parts, one coming from the single-particle excitation and the other from plasmon excitation.

Early electron scattering experiments² confirmed the existence of plasmon excitation and hence the validity of the RPA theory. Nevertheless small deviations from RPA predictions in the range of small momentum transfer were observed. The main points of these discrepancies are (i) the experimentally deduced dispersion curve falls lower than RPA predictions, and (ii) the width

of the experimentally observed plasmon excitation is larger than theoretically predicted. This implies the existence of some damping mechanism for $k < k_c$ which is not included in the RPA theory.

X-ray experiments have also confirmed the existence of plasmon excitation and the validity of RPA.⁴ However subsequent experiments^{5,6} showed considerable disagreements with RPA predictions. The most important was the persistence of plasmons far beyond the critical wave vector k_c and a double-peak structure. Further experimental work⁶⁻⁹ confirmed the inadequacy of RPA in the region of intermediate and large momentum transfer.

The above experimental findings are common to such diverse systems as Al, Be, C, and Li, indicating that they result from the properties of the conduction-electron gas rather than from different band structures.⁶ Furthermore, calculations within the framework of RPA considering band-structure effects⁷ have shown that such effects will modify, even in the most favorable case, the free-electron spectrum of simple metals by a few percent.

Thus the failure of RPA to describe experimental results in the region of intermediate and large momentum transfer, was attributed to the fact that short-range electron correlation effects are ignored within that approximation.^{1,3} Many authors¹⁰⁻¹² have attempted, without total success, to reproduce the experimental results by extending the RPA with the inclusion of short-range correlation effects and some damping mechanism.

Experiments using x-ray scattering⁸ showed that plasmon excitations in lithium continue all the way through the particle-hole continuum and that a second peak appears for high k . In other experimental work on beryllium⁹ it has been shown that in addition to the persistence of plasmons above k_c , there is a flattening in the dispersion curve (for $k > k_c$) which then continues with a negative slope.

The above features could not be explained in the context of the post-RPA theories. However it is interesting to note that the negative slope may suggest the possibility of bound-plasmon formation¹³ or superfluid heliumlike behavior of the electron gas,¹⁴ as has been proposed in different theoretical approaches.

Therefore it was considered necessary to carry out measurements for the determination of the dynamic structure factor $S(\mathbf{k}, \omega)$ in order to verify previous observations, extend them over a large region of transferred momentum k and examine the shape of $S(\mathbf{k}, \omega)$ in this region, obtain a more complete picture of the dispersion curve, and finally compare these experimental results with existing theories.

EXPERIMENTAL DETAILS AND RESULTS

The energy analysis of scattered x-ray radiation is accomplished with the aid of a horizontal x-ray spectrometer which has been constructed to meet the specific requirements of the present work. This is essentially a Joha-type curved-crystal spectrometer and is an improved version of similar instruments described elsewhere.^{4,15}

The layout of this spectrometer is shown schematically in Fig. 1. A quartz single crystal cut along the [2243] direction is used as the analyzing crystal (AC). Polycrystalline Be was used as the scatterer (S). However, in order to measure in regions in which Bragg reflections were prominent, two Be single crystals cut parallel and perpendicular to the c axis, respectively, were used. The scatterer (S) was placed inside the focusing circle and was bent as indicated in Fig. 1. Due to this geometry the scattering angle is determined with high accuracy depending only upon the scatterer thickness. In the present work the thickness of all the samples was about 2 mm. This implies an error in the scattering angle of $\pm 0.5^\circ$. The transferred momentum k is related to the scattering angle ϕ and the wavelength of the incident beam

$$k = (4\pi/\lambda)\sin(\phi/2),$$

and thus the resulting error in the transferred momentum k is $\pm 0.03 \text{ \AA}^{-1}$. In order to avoid x-ray scattering and absorption by air, the samples were mounted in a vacuum chamber. For the same reason most of the path of the scattered beam was through evacuated tubes. With the

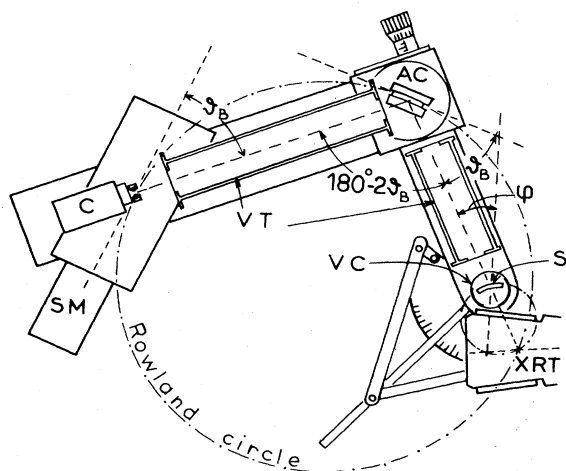


FIG. 1. Lay out of the horizontal x-ray spectrometer. XRT, position of the x-ray tube. S, scatterer; VC, vacuum chamber; VT, vacuum tubes; AC, analyzing crystal; C, counter; SM, step motor.

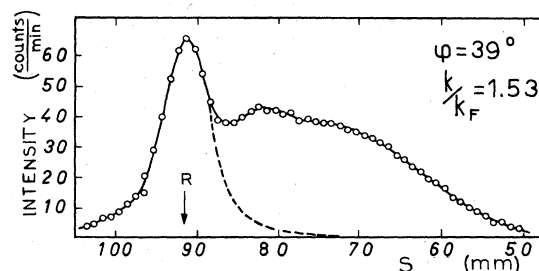


FIG. 2. Typical spectrum of the inelastically scattered radiation.

aid of a rotary transmission attachment the sample was rotated about a vertical axis to $\phi/2$ when the scattering angle changes by ϕ . This is necessary in order to have the same error at all scattering angles. A copper anticathode x-ray tube was used, operated at 60 kV and 30 mA. The spectrometer was adjusted to the spectral region near the Cu $K\beta$ line which is used as the primary beam. The use of a single line instead of the more intense doublet Cu $K\alpha_1\alpha_2$ is preferred due to the undistorted spectrum obtained with the singlet as discussed elsewhere.^{8,9} The full width at half maximum (FWHM) of the primary beam is 8.1 eV, including the 5.84 eV natural width of Cu $K\beta$ line,¹⁶ resulting in a resolving power of 1095. The analog detector is fixed on a remote-controlled table, permitting micrometric positioning of the detector, which moves along the Rowland circle as indicated in Fig. (1). At each scattering angle the intensity of the scattered radiation is recorded by the counter for each micrometric reading of the detector position. It is a simple matter to convert the distance scale to an energy scale.

Figure 2 shows a typical spectrum (raw data) of scattered radiation from polycrystalline beryllium. The scattering angle is 39° corresponding to $k = 1.53k_F$, where k_F is the Fermi wave vector. The open circles in Fig. 2 (and in Fig. 3) are drawn to incorporate the statistical error. The position of the maximum elastic component is marked with R. The background has been subtracted and the remaining spectrum has also been corrected for absorption. The spectrum thus obtained contains both elastic and inelastic components of the scattered radiation. The elastic component (Fig. 2, dashed line) is obtained by a standard procedure with the aid of a "dummy experiment" described elsewhere.⁴ Subsequently this elastic component was subtracted from the measured spectrum and thus the inelastic component is obtained.

Figure 3 shows the resulting inelastic component of eight out of twenty-six of the measured spectra for characteristic regions of momentum transfer, as indicated at the upper corner of each spectrum. The y axis represents the intensity of the spectrum normalized to unity, while the x axis represents the energy loss in eV units of the inelastically scattered x-ray photons. The inelastic component is the interesting part of the spectrum, as it is directly related to the dynamic structure factor $S(\mathbf{k}, \omega)$. The structure factor has also been calculated within the RPA approximation. The result has been convoluted with the elastic component of the scattered radiation and has

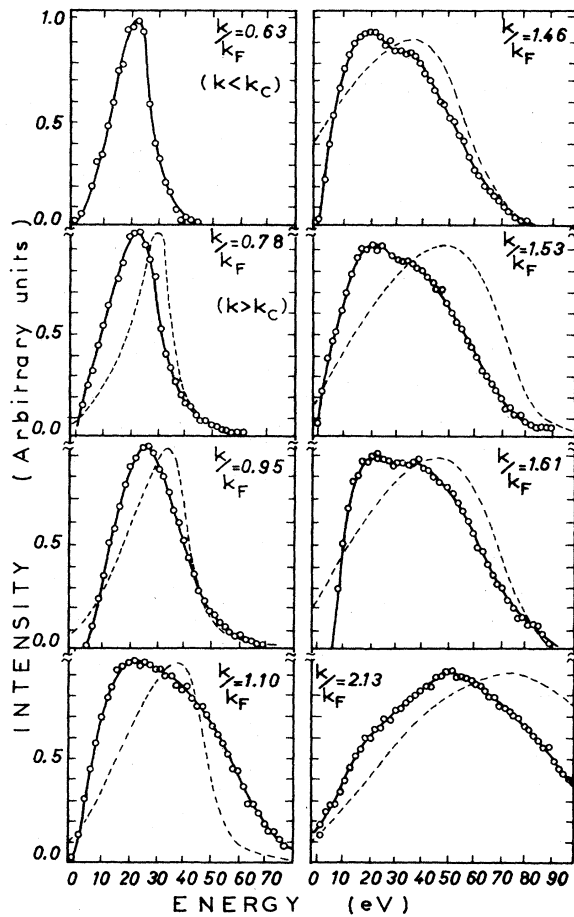


FIG. 3. Dynamic structure factor spectra as a function of energy for different regions of transferred momentum k .

been plotted with a dashed line in the corresponding spectra of Fig. 3. The discrepancy between RPA theory and experimental results is obvious.

The essential features of $S(\mathbf{k}, \omega)$, as shown in Fig. 3, are as follows.

(i) For k values less than k_{FT} (where $k_{FT} = 1.1k_F$), it is clear that the position of the maximum in $S(\mathbf{k}, \omega)$ shifts towards higher energy as the transferred momentum k approaches k_{FT} .

(ii) For k values greater than k_{FT} , a shoulder appears in the high-energy region which becomes more pronounced as k increases. Indeed, as k increases the shoulder first resolves into a second peak and finally, at sufficiently high k , the higher-energy peak dominates the spectrum.

(iii) The peak shape varies such that the (FWHM) intensity increases with k .

Figure 4 shows the dispersion curve which represents the variation of the energy of the peak in $S(\mathbf{k}, \omega)$ with transferred momentum k . For the purpose of clarity the vertical scale has been normalized with $\hbar\omega_p$, which is the plasmon energy corresponding to $k=0$, and the horizontal scale normalized with k_F . The boundaries A and B indicate the region within which single-particle excitation is expected. For comparison, the dispersion curve corre-

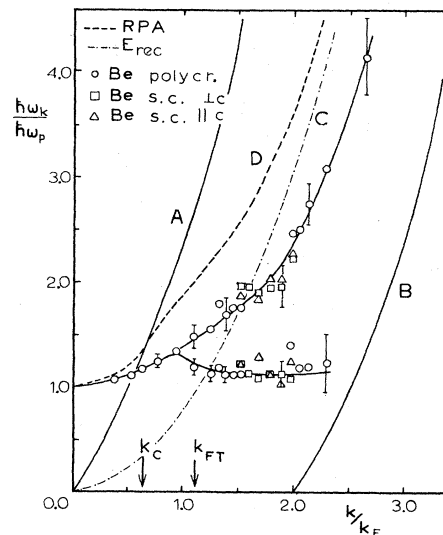


FIG. 4. Dispersion curve of $S(\mathbf{k}, \omega)$ maxima. Curves A and B are the continuum limits.

sponding to free-electron recoil is shown as curve C while curve D is the dispersion curve predicted by RPA. The experimental curve of Fig. 4 shows the following interesting features.

(i) The region of $k < k_c$ where there is a lowering of the dispersion curve relative to the RPA predicted curve.

(ii) Plasmonlike component persists for $k > k_c$, and at $k \approx k_{FT}$ the dispersion curve splits into two branches.

(iii) The lower branch corresponds to a plasmonlike component. A negative slope is observed in the region of $0.9k_F < k < 1.5k_F$, while for greater values of k it remains almost nondispersive until the continuum limit has been reached.

(iv) The upper branch, which corresponds to the second peak that appears in $S(\mathbf{k}, \omega)$, shows considerable dispersion and for large values of k tends to become parallel to the recoil energy curve C .

The FWHM intensity of the observed spectra $S(\mathbf{k}, \omega)$ is shown in Fig. 5 as a function of the momentum transfer, in units of k_F (quadratic scale). In the same figure the FWHM of $S(\mathbf{k}, \omega)$, predicted by RPA theory after convolution with the primary-radiation spectrum, is also plotted. It is apparent that there is a discontinuity for $k = k_c$ in agreement with previous experiments using fast electrons.¹⁷

DISCUSSION

The purpose of this discussion is to compare the observed dispersion curves, with currently available theoretical models and experimental results of other workers.^{6,8,9,18,19} Considering, first of all, the dispersion curve (Fig. 4), for $k < k_c$, it can be said that basically there is an agreement between the results of the present work and with previous experimental results^{6,9} as well as the RPA theory, if corrections for short-range correlations are taken into account.

Furthermore, in the region of $k_c < k < k_F$ the plasmon-

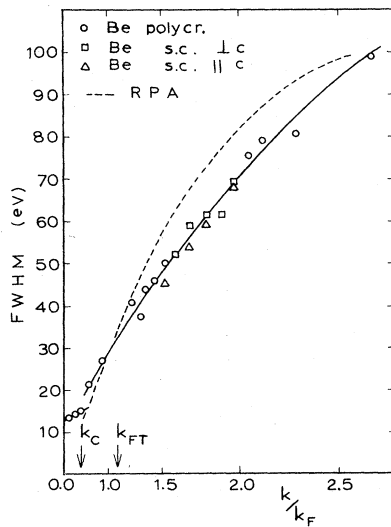


FIG. 5. Full width at half the maximum intensity of the $S(\mathbf{k}, \omega)$ spectra vs the momentum transfer.

like component persists in the excitation spectrum (Fig. 4). However, it should be remarked that the experimental appearance of $S(\mathbf{k}, \omega)$ for values of k around k_c hardly justifies the distinction in interpreting the peak as plasmon or "plasmonlike." This statement is reinforced by reference to the spectra for $k = 0.63k_F$ and $k = 0.78k_F$ (Fig. 3), where the second high-energy peak is insignificant. Therefore the critical wave vector k_c must not be considered as a sharp limit below which plasmons exist while beyond this limit they disappear, but rather as defining the onset of the region of stronger plasmon damping. This is also supported from the discontinuity observed for $k = k_c$ in the FWHM curve (Fig. 5). It is also apparent, from Fig. 5, that there is a linear dependence of FWHM with k^2 for $k < k_c$, while for $k > k_c$ additional terms seem to be present. In the region of $k > k_{FT}$ the experimental curve lies below the theoretical curve (dashed line in Fig. 5) and this means that RPA predicts stronger damping effects than required for the interpretation of our data.

In the region of $k_F < k < 1.5k_F$ the dispersion curve (Fig. 4) shows a negative slope. In the same region the appearance of a second peak begins. These results are in very good agreement with our previous results on beryllium⁹ and consistent with the results of other experimental work using x rays.⁶

As was mentioned, in the region of $k > 1.5k_F$, the plasmonlike component is nondispersive while the upper branch is strongly dispersive tending to become parallel to the recoil energy curve. These features have also been observed in the case of lithium.⁸

In previous electron scattering experiments¹⁸ for $k > k_F$ a second branch was not observed in the dispersion curve while the experimental points seem to follow the upper branch of the dispersion curve presented here. This disagreement is probably due to the fact that electron scattering experiments are less appropriate in this region of intermediate and large momentum transfer k , as point-

ed out and discussed in detail elsewhere.⁹

Quite recently Schulke *et al.*¹⁹ reported that the double-peak structure of $S(\mathbf{k}, \omega)$ in Li "seems not to be a universal property of the strongly correlated gas" and "apparently has its origin in the band structure." They interpreted their results with the two-band model theory of E-Ni Foo *et al.*²⁰ However, in a later paper,⁷ it was shown that the above-mentioned model has "several unusual and unrealistic features" and concluded, as was mentioned in the Introduction, that band-structure effects modify by a few percent the free-electron spectrum. The only available full band-structure calculation of the $S(\mathbf{k}, \omega)$ by Taut and Hanke,²¹ revealed a double-peak structure for $k > k_c$ for Be. However, there is a disagreement among this calculation, our results, and the results of a two-band model,²⁰ regarding the peak energies and separation of the peaks in the doublet structure of what they call "collective band-structure peak." This fact, along with the fact that it is hard to understand boundary collective excitation⁷ for $k_c < G/2$ (G a reciprocal-lattice vector), lead to the conclusion that, at least in the case of Be, where for all directions $k_c < G/2$, the double-peak structure is due to electron-correlation effects.

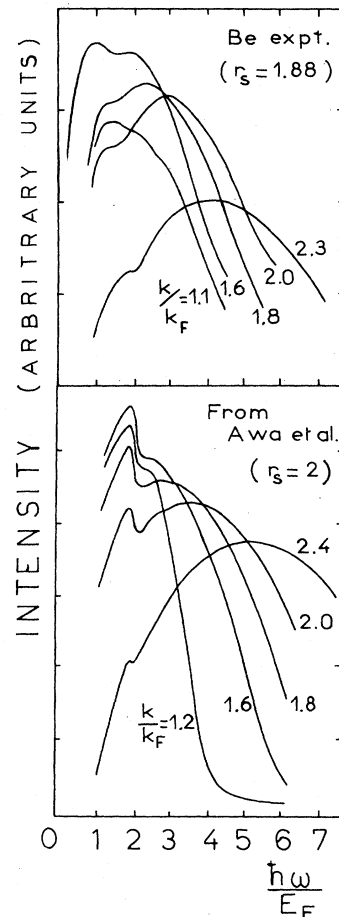


FIG. 6. Shape of $S(\mathbf{k}, \omega)$ for different transfer momentum as experimentally determined in the present work and calculated from the theory of Awa *et al.* (Ref. 26).

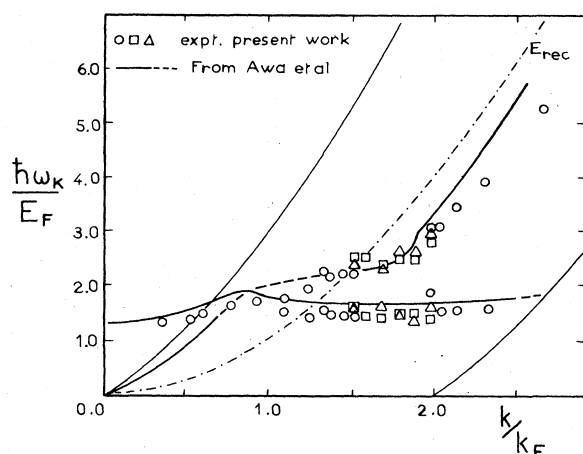


FIG. 7. Dispersion curve of $S(k, \omega)$ maxima. Solid and dashed lines correspond to the theory of Awa *et al.* (Ref. 26) while points are from present experimental work.

The existing post-RPA theories, those using the techniques of decoupling terms of higher order from kinetic equations for Wigner distribution functions,^{10,12,22} have not succeeded in predicting the double-peak structure in $S(k, \omega)$ which is established experimentally. By introducing lifetime effects, Mukhopadhyay *et al.*²³ were able to reproduce the double structure, but the agreement with experiment was poor. De Raedt and De Raedt²⁴ obtained a double-peak structure using the Mori formalism, but they were forced to introduce arbitrary parameters without any obvious physical meaning in order to fit their theory with the experimental data. Using diagrammatic techniques, Green *et al.*²⁵ had also obtained a double-peak structure in $S(k, \omega)$ but without much success in fitting the experimental data. Awa *et al.*,²⁶ using the same techniques and on the basis of the quasi-one-pair excitation approximation, achieved a very good agreement with experimental results on lithium.⁸

The results of the present work show also an excellent agreement with the work of Awa *et al.*²⁶ In Fig. 6 the experimentally deduced shape of $S(k, \omega)$ and the calculated forms by Awa *et al.*²⁶ are shown for comparison. The coincidence is remarkable considering that the calculated spectra are not convoluted with the spectrum of primary beam (the convolution should broaden the spectra).

The theoretical work of Awa *et al.*²⁶ calculates the dispersion curve and, most significantly, this shows two branches, one corresponding to the plasmonlike component (lower branch) and the other to the single-particle excitation spectrum (upper branch) which shows strong dispersion. It is worth mentioning that this theory is the only one clearly predicting the existence of a double-branch dispersion curve and a negative slope for the plasmonlike component. It is remarkable that the experimentally observed negative slope in the region of $0.9k_F < k < 1.5k_F$, reported in this paper and elsewhere,⁹ appears almost exactly in the same region as the one predicted by the theory of Awa *et al.*²⁶ ($0.8k_F < k < 1.4k_F$). For comparison, in Fig. 7, the theoretical dispersion curve from the above-mentioned theory has been plotted together with the experimental points resulting from the present work.

Many theories incorporate exchange and short-range correlation effects in order to reproduce the experimental results. However, the manner in which short-range effects are taken into account is most important for the success of the theory in agreeing with the experimental data. On the basis of the above-mentioned coincidence between the theory of Awa *et al.*²⁶ and the results of the present work, it is concluded that the procedure which this theory uses to take into account electron correlation is the most successful.

In conclusion, the observed discrepancies between experimental results and RPA theory can be attributed, according to the theory of Awa *et al.*²⁶ to short-range correlation effects and the existence of higher-order excitations such as two-pair excitation and one-pair plasmon excitation.

¹D. Pines, *Elementary Excitations in Solids* (Benjamin, New York, 1964).

²H. Raether, in *Excitation of Plasmons and Interband Transitions By Electrons*, Vol. 88 of *Springer Tracts in Modern Physics*, edited by G. Honler (Springer, Berlin, 1980).

³For a review article, see S. Ichimaru, *Rev. Mod. Phys.* **54**, 1017 (1982).

⁴G. D. Priftis, *Phys. Rev. B* **2**, 54 (1970).

⁵D. M. Miliotis, *Phys. Rev. B* **3**, 701 (1971).

⁶P. Eisenberger, P. M. Platzman, and K. C. Padney, *Phys. Rev. Lett.* **31**, 311 (1973); P. M. Platzman and P. Eisenberger, *ibid.* **33**, 152 (1974); P. Eisenberger, P. M. Platzman, and P. Schmidt, *ibid.* **34**, 18 (1975); P. Eisenberger and P. M. Platzman, *Phys. Rev. B* **13**, 934 (1976).

⁷K. C. Pandey, P. M. Platzman, P. Eisenberger, and E-Ni Foo, *Phys. Rev. B* **9**, 5046 (1974).

⁸G. D. Priftis, J. Boviatsis, and A. Vradis, *Phys. Lett.* **68A**, 482 (1978).

⁹G. D. Priftis and J. Boviatsis, *Phys. Status Solidi B* **104**, 673 (1981).

¹⁰P. Vashishta and K. S. Singwi, *Phys. Rev. B* **6**, 875 (1972).

¹¹A. Holas, P. K. Aravind, and K. S. Singwi, *Phys. Rev. B* **20**, 4912 (1979).

¹²J. T. Devreese, F. Brosens, and L. F. Lemmens, *Phys. Status Solidi B* **91**, 349 (1979); *Phys. Rev. B* **21**, 1349 (1980); **21**, 1363 (1980).

¹³J. Ruvalds, A. K. Rajagopal, J. Carballo, and G. S. Grest, *Phys. Rev. Lett.* **36**, 274 (1976).

¹⁴P. M. Platzman and P. Eisenberger, *Solid State Commun.* **14**, 1 (1974).

¹⁵W. Schulke, U. Berg, and O. Brummer, *Phys. Status Solidi B* **35**, 227 (1969).

¹⁶G. Brogen, *Ark. Fys.* **23**, 219 (1962).

¹⁷P. C. Gibbons, S. E. Schnatterly, J. J. Ritsko, and J. R. Fields, *Phys. Rev. B* **13**, 2451 (1976).

¹⁸P. E. Batson, C. H. Chen, and J. Silcox, *Phys. Rev. Lett.* **37**,

- 937 (1976); C. H. Chen, A. E. Meixner, and B. M. Kincaid, *ibid.* **44**, 951 (1980).
- ¹⁹W. Schulke, H. Nagasawa, and S. Mourikis, *Phys. Rev. Lett.* **52**, 2065 (1984).
- ²⁰E-Ni Foo and J. J. Hopfield, *Phys. Rev.* **173**, 635 (1968).
- ²¹M. Taut and W. Hanke, *Phys. Status Solidi B* **77**, 543 (1976).
- ²²K. Utsumi and S. Ichimaru, *Phys. Rev. B* **22**, 1522 (1980); **22**, 5203 (1980); **23**, 3291 (1981).
- ²³G. Mukhopadhyay, R. K. Kalia, and K. S. Singwi, *Phys. Rev. Lett.* **34**, 950 (1975).
- ²⁴H. De Raedt and B. De Raedt, *Phys. Rev. B* **18**, 2939 (1978).
- ²⁵F. Green, D. N. Lowry, and J. Szymanski, *Phys. Rev. Lett.* **48**, 638 (1982).
- ²⁶K. Awa, H. Yasuhara, and T. Asahi, *Solid State Commun.* **38**, 1285 (1981); *Phys. Rev. B* **25**, 3670 (1982); **25**, 3687 (1982).